Directional Analysis of Vehicle-to-Vehicle Propagation Channels

Abbas, Taimoor; Kåredal, Johan; Tufvesson, Fredrik; Paier, Alexander; Bernadó, Laura; Molisch, Andreas

Published in:
IEEE Vehicular Technology Conference

2011

Directional Analysis of Vehicle-to-Vehicle Propagation Channels

Taimoor Abbas*, Johan Karedal*, Fredrik Tufvesson*, Alexander Paier†, Laura Bernadó‡, and Andreas F. Molisch§
*Dept. of Electrical and Information Technology, Lund University, Lund, Sweden
†Institute of Telecommunications, Vienna University of Technology, Vienna, Austria
‡Forschungszentrum Telekommunikation Wien (FTW), Vienna, Austria
§Dept. of Electrical Engineering, University of Southern California, Los Angeles, CA, USA

***Abstract*—This paper presents a double directional analysis of vehicle-to-vehicle channel measurements conducted in three different traffic scenarios. Using a high-resolution algorithm, we derive channel parameters like Angle-of-Arrival (AOA), Angle-of-Departure (AOD), propagation delay and Doppler shift and identify underlying propagation mechanisms by combining these estimates with maps of the measurement sites. The results show that first-order reflections from a small number of interacting objects can account for a large part of the received signal in the absence of line-of-sight (LOS). This effect is especially pronounced in the two traffic scenarios where the road is not lined with buildings. We also found that the direction spread is low (and conversely that the antenna correlation is high) in such scenarios, which suggests that beam forming rather than diversity-based methods should be used if multiple antenna elements are available. The situation is reversed, however, in the third scenario, a narrow urban intersection, where a larger number of higher-order reflections is found to result in a higher direction spread.**

I. Introduction

Vehicle-to-vehicle (V2V) communication systems have attracted a lot of interest in recent years due to their anticipated usefulness for traffic safety enhancement. Particularly, it is envisioned that future vehicles, equipped with radio transceivers, can share information about traffic dynamics with each other in order to facilitate driving and avoid accidents. Since the efficiency and the accuracy of such systems ultimately depends on the properties of the propagation channel, a lot of research effort has been spent on V2V propagation channels, usually with the intent of developing realistic simulation models (see e.g., [1], [2], [3]).

Although a number of propagation channel measurement campaigns have been performed in recent years (see e.g., [4], [5], [6], [7]), there are still many important aspects that have been little explored. First, the antenna impact is not well understood. Almost exclusively, the measurements conducted so far have been done with "regular" antenna arrays placed at an elevated position (above the vehicle roof). Neither the impact of design constraints nor antenna placement has been given much attention. Secondly, most measurement campaigns have been conducted under "general" traffic conditions, with cars driving either in convoy or in the opposite directions on the same road, e.g., on highways [4], [5] (a recent is found in [8], where signal obstruction due to vehicles is analyzed). In addition to such general traffic situations there are a number of *application-specific* scenarios where special propagation conditions apply, e.g., collision avoidance scenarios in street intersections or traffic congestion scenarios. These conditions are not well captured by the former standard measurement scenarios, and hence separate characterization of such scenarios is required.

Furthermore there is a lack of available results on directional properties of V2V channels in the literature; to the authors' best knowledge there is only the paper by Pedersen et al., [9], which presents the angular spectra for convoy measurements. Analysis of directional properties is important for the assessment of multi-antenna capabilities, e.g., for evaluating the possible diversity gain, as well as to improve understanding of important propagation effects.

The current paper addresses these gaps of knowledge by presenting the results of extensive multiple-input multiple-output (MIMO) V2V channel measurements performed in Lund, Sweden. We present results of directional analysis for three *application-specific* scenarios and use these results to identify the underlying propagation mechanisms and analyze their impact on the total received power. We also evaluate the directional spread of the propagation channels in the different scenarios, and derive antenna correlation coefficients. The scenarios we study are: (i) an intersection scenario, (ii) a congestion scenario, and (iii) a controlled line-of-sight (LOS) obstruction between the vehicles moving on a highway. This paper partly extends the results of [10], where we presented power-delay profiles and root mean square (RMS) delay spreads (but no directional results) for different types of intersections.

The paper is organized as follows: In Section II the measurement setup is described in detail and the properties of three different scenarios are explained. The parameter extraction process is described in Section III, whereas the results, including the identified propagation mechanisms, are presented in Section IV. Finally, the summary and conclusions are presented in Section V.

This work was partially funded by the Vienna Science and Technology Fund (WWTF) in the FTW project COCOMINT, partially by the SSF center for High-Speed Wireless Communication and was carried out in cooperation with the FTW project ROADSAFE and the Christian Doppler Laboratory for Wireless Technologies for Sustainable Mobility.

978-1-4244-8329-7/11/$26.00 ©2011 IEEE

II. Channel Measurements

A. Measurement Setup

V2V channel measurement data were recorded using the RUSK Lund channel sounder that performs switched-array MIMO measurements. The measurements were conducted over a 240 MHz bandwidth centered around 5.6 GHz, the highest allowed center frequency of the sounder. The measurements were performed using standard hatch-back style cars with roof mounted four-element antenna arrays, specifically designed for V2V communication [11]. The antenna height was 1.73 m. For each branch of this 4×4 MIMO configuration, the channel sounder sampled the complex time varying channel transfer function $H(f,t)$ every $\Delta t = 307.2\,\mu$s during 10 or 20 s. To keep track of the positions of the transmitter (TX) and and receiver (RX) vehicles during the measurements, each vehicle logged the GPS coordinates and had videos, taken through the windshield. These data were also combined with the measurement data, in order to identify important scatterers in the post-processing.

B. Measurement Scenarios

The measurement data we study were collected in different traffic scenarios.

In the first scenario (intersection) the TX and RX, were approaching a four way intersection in an urban environment at a speed of $30-40$ km/h ($8-11$ m/s); see Fig. 1(a). There were houses on both sides of the streets, which obstructed the LOS until the cars met in the intersection (in practice, the TX car stopped at a yield sign while the RX car drove by). The streets were narrow; the street width was $14-18$ m. Moreover, there were several street lights and road signs in this scenario, and many parked cars along the streets, but few moving vehicles.

In the second scenario (congestion) the TX car had just entered a congested area on a two-lane highway (due to a road works further ahead forcing the two lanes to merge). The TX car was stuck in the right lane whereas the RX car was approaching from behind in the left lane at a speed of about 70 km/h (20 m/s); see Fig. 1(b). There were road signs, light poles, various objects and a multitude of other vehicles in this scenario; beside the large number of cars standing still in the TX/RX direction, there was also (moving) traffic in the opposite direction, including some trucks. There was a metallic fence on the outer (right) boundary of the road and the directions of travel were separated by a low concrete wall (approximately 0.5 m).

In the third scenario (obstructed-LOS) the TX and RX cars were moving in the same direction on the right lane on a two-lane highway at a speed of 110 km/h (30 m/s); see Fig. 1(c). There were trucks in front of as well as behind the TX/RX convoy, and the LOS path was obstructed by a tall van between TX and RX. The LOS path appeared when the van decided to change lanes. There were many vehicles (moving) in the opposite direction and there were a couple of road signs and overhead electrical power transmission lines with poles on the roadside. Finally, the directions of travel were separated by a low metallic fence.

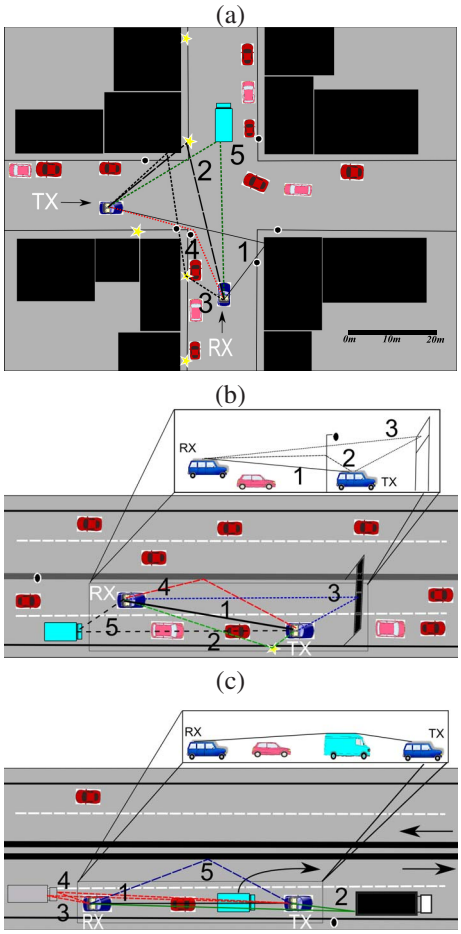

Fig. 1. Identified propagation mechanism behind the five strongest MPCs at a particular instant t, for the (a) intersection ($t = 6$ s); (b) congestion ($t = 13$ s) and (c) obstructed LOS ($t = 1$ s) scenarios. Stars, dots, blocks and dark strip represent streetlights, roadsigns, houses and concrete wall/metallic fence that separates the direction of travel on the highway, respectively.

III. Parameter Extraction

We assume that the 4×4 channel matrix $\mathbf{H}$ can be described by a sum of L plane waves or multipath components (MPCs) where each wave l is characterized by a complex amplitude γ_l, propagation delay τ_l, and a Doppler shift ν_l. We then model the channel transfer function at each temporal instant (snapshot) t_s and frequency point f_k by [12]

$$\mathbf{H}[t_s,f_k] = \sum_{l=1}^{L} e^{j2\pi\nu_l t_s} \begin{bmatrix} g_{TX}^H(\Theta_{TX,l}) & g_{TX}^V(\Theta_{TX,l}) \end{bmatrix} \cdot \begin{bmatrix} \gamma_l^{HH} & \gamma_l^{HV} \\ \gamma_l^{VH} & \gamma_l^{VV} \end{bmatrix} \begin{bmatrix} g_{RX}^H(\Theta_{RX,l})^T \\ g_{RX}^V(\Theta_{RX,l})^T \end{bmatrix} e^{-j2\pi\tau_l f_k}, \tag{1}$$

where $\mathbf{H} \in \mathbb{C}^{4\times4}$; g_{TX}^H, g_{TX}^V and g_{RX}^H, g_{RX}^V are 4×1 complex vectors representing TX and RX antenna responses, respectively. Furthermore, $\Theta_{TX,l} = (\theta_{TX,l}, \phi_{TX,l})$, $\Theta_{RX,l} = (\theta_{RX,l}, \phi_{RX,l})$ are angle-of-departure in elevation and azimuth, and angle-of-arrival in elevation and azimuth, respectively. Superscript H and V indicate horizontal and vertical polarization, respectively.

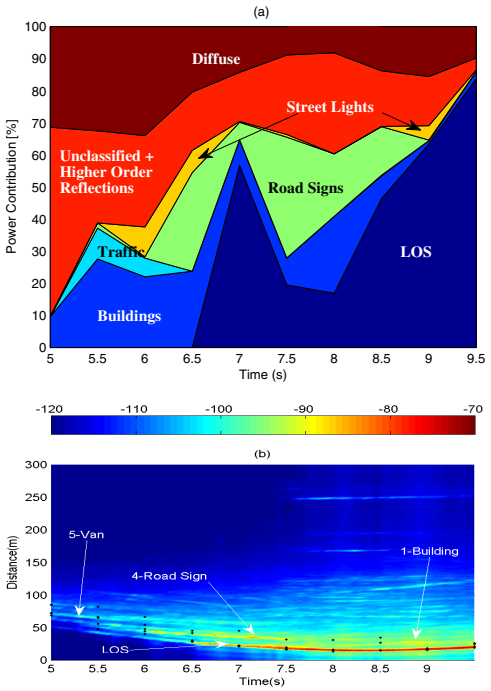

Fig. 2. Results for the intersection scenario: (a) shows the relative power contribution from different propagation mechanisms, only LOS and first-order reflections are categorized explicitly; (b) shows some identified propagation mechanisms in the time-delay domain (power-delay profile), dots indicate the SAGE delay estimates for the five strongest MPCs.

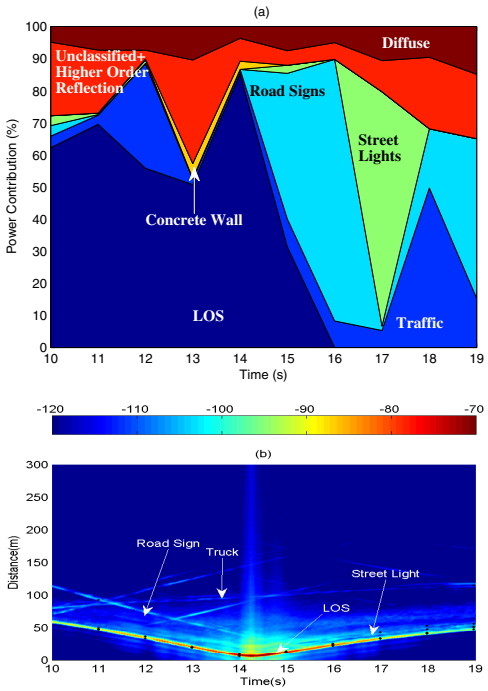

Fig. 3. Results for the congestion scenario: a) shows the relative power contribution from different propagation mechanisms, only LOS and first-order reflections are categorized explicitly; (b) shows some identified propagation mechanisms in the time-delay domain (power-delay profile), dots indicate the SAGE delay estimates for the five strongest MPCs.

The parameters of (1) for 50 MPCs are estimated using the space-alternating generalized expectation-maximization (SAGE) algorithm [13]. In order to reduce the computational complexity, we use measurement data with a bandwidth of 20 MHz, out of the full 240 MHz, centered around 5.6 GHz, and a temporal window of length 19.4 ms (64 snapshots). This temporal window corresponds to a Doppler resolution of 52 Hz and is selected based on the estimated stationarity time of the channel (see [14] for details), which is 97.6 ms, 374.4 ms, and 1337.9 ms for the intersection, congestion and obstructed-LOS scenarios, respectively. Due to the computational efforts of estimating parameters using SAGE, we limit the analysis to a temporally sparse subset of the measurements data; every 0.5 s in the intersection, every 1 s in the other two. The 50 extracted MPCs account for $68-90\%$, $83-98\%$ and $68-94\%$ of the available power in the intersection, congestion and obstructed-LOS scenarios, respectively. For this power percentage evaluation, the mean squared amplitude of the inverse Fourier transform of, the measured and the reconstructed, channel transfer functions were noise thresholded, i.e., anything below noise floor with an additional 3 dB margine was considered as noise and thus set to zero. We label the fraction of power which is not extracted by SAGE as *diffuse* power, though strictly speaking this part also contains measurement noise. Moreover, the extracted part may also contain diffuse contributions to some extent (for those time instants where the selected source order is too high); this will be discussed further in the paper. The percentage of extracted power is generally lower for instants where non-LOS conditions apply.

IV. Results

For each scenario and each time instant we plot the estimated propagation paths on the corresponding site maps and then perform a measurement based ray-tracing from the TX and RX, in order to identify the underlying propagation mechanisms, e.g., if an object is found at (or more specifically "sufficiently close" to) the intersection of the lines drawn in the direction of the AOA from the RX and the direction of the AOD from the TX for a certain MPC, and the geometric length from TX to RX via this intersection matches the delay estimate for the MPC, we consider a single-bounce reflection from that object to be the underlying mechanism behind it. In this process, the coordinates of the TX and RX are determined by combining recorded GPS and video data, whereas the coordinates of moving scatterers are determined using video data only. Obviously, only the coordinates of moving scatterers within the visibility range of the TX and RX can be determined, and the accuracy of their coordinates depends on their position relative to the TX and/or RX. Although a small discrepancy between the coordinates of an actual object and the location indicated by the estimated parameters is inevitable due to errors in the positions of the TX and RX cars, we are able to identify the likely propagation process in the vast majority of the cases. We are further aided in the identification process by the Average Power Delay Profiles (APDPs), which are defined, for each time instant, as the averaged (over the 4×4 MIMO branches) squared magnitude of inverse Fourier transform of the channel transfer function at that instant. Many important MPCs show up as "lines" in the APDP, and the

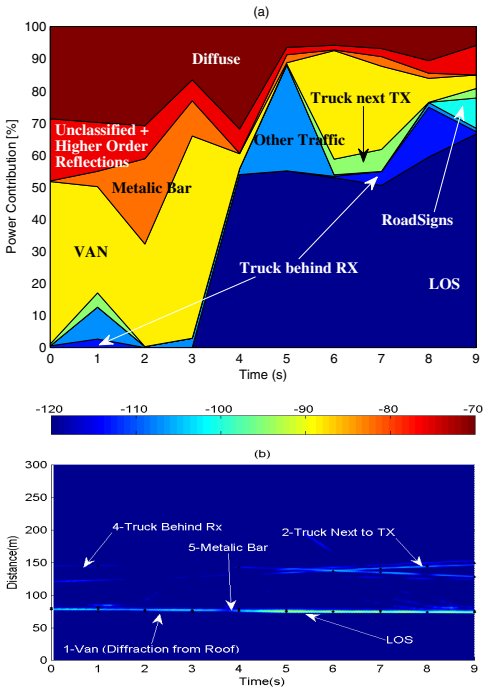

Fig. 4. Results for the general LOS-obstruction scenario: a) shows the relative power contribution from different propagation mechanisms, only LOS and first-order reflections are categorized explicitly; (b) shows some identified propagation mechanisms in the time-delay domain (power-delay profile), dots indicate the SAGE delay estimates for the five strongest MPCs.

APDP can therefore be used to assess the temporal evolution of the propagation delay of those MPCs. APDPs for the three scenarios are shown in Fig. 2, 3, and 4, respectively. It is important to mention that the SAGE for some reasons cannot subtract the LOS completely and model the residue as specular paths. These paths cannot be tied to any of the described propagation mechanism and thus regarded as unclassified.

Sample plots of the identified MPCs at a certain time instant are shown in Fig. 1. As an example of the identification process, consider MPC#5 in the intersection scenario in Fig. 1(a). This MPC is arriving at the RX from a direction where the only physical object is another vehicle (a van). In some cases, such as MPC#3, the interacting objects cannot be identified for certain, but we can say with high probability that a single-bounce process is *not* the underlying mechanism. Similarly in the congestion scenario (Fig. 1(b)), where there is a multitude of traffic around the TX/RX we can still identify important propagation mechanism, e.g., MPC#2 which is a street light, using the fact that it is only object in the estimated direction and that the measured geometric distance also matches the estimated delay. As a final example, consider MPC#3 and MPC#4 in the obstructed LOS scenario (Fig. 1(c)). We conclude that they both stem from same object, a truck behind the RX, since they have very similar AOAs and AODs. There is, however, a small difference in the propagation distance which indicates the possibility that one signal is reflected from the bonnet whereas the other stems from the body of the truck.

Once the identification process is complete, we classify the propagation mechanisms into two different categories: the

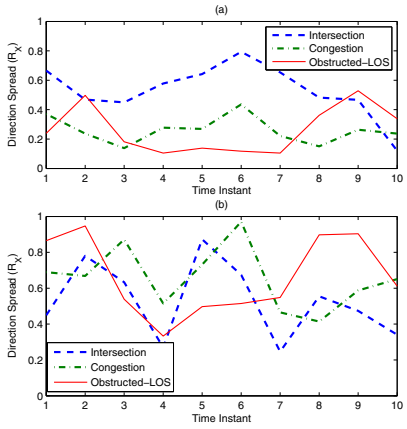

Fig. 5. RMS direction spread at RX: (a) with antenna influence; (b) without antenna influence.

LOS path, single-bounce interactions (with buildings, traffic, road signs, street lights, and parked cars, and the concrete wall/metallic fence that separates the directions of travel on the highway) are used in all scenarios. In the obstructed-LOS scenario we split the traffic category into three sub-categories: trucks in front and behind the TX/RX, a van between the TX/RX and other traffic. Lastly, we use a category labeled "unclassified plus higher order reflections account" for both higher-order reflections and for the MPCs that cannot be tied to a specific propagation mechanism. This category will also contain a small amount of diffuse power extracted by SAGE.

Before we study how the received signal is composed, we add antenna influence to the extracted path weights. This way, the weights can be related to the energy that is *not* extracted by SAGE (see Section III). We thus have:

$$\alpha_l = \Bigg| \sum_k g_{TX}^H \diamond \begin{bmatrix} g_{RX}^H & g_{RX}^V \end{bmatrix} \begin{bmatrix} \gamma_l^{HH} \\ \gamma_l^{HV} \end{bmatrix} + g_{TX}^V \diamond \begin{bmatrix} g_{RX}^H & g_{RX}^V \end{bmatrix} \begin{bmatrix} \gamma_l^{VH} \\ \gamma_l^{VV} \end{bmatrix} \Bigg|^2, \tag{2}$$

where, $\gamma_l^{HH}, \gamma_l^{VV}$ and $\gamma_l^{VH}, \gamma_l^{HV}$ represent the the co-polarized and cross-polarized estimated complex path gains of extracted MPCs, respectively whereas the variable k and the operator $\diamond$ refer to the number of channels and the Khatri-Rao product respectively. Finally, the contribution from each propagation mechanism in total received power is calculated as,

$$P_j = \frac{\sum_{l \in S_j} \alpha_l}{\sum_l^L \alpha_l}, \tag{3}$$

where P_j is the power contribution corresponding to the j^{th} MPC category S_j. The results (see (a) of Fig. 2, 3,and 4) show that first-order interactions often dominate in the absence of LOS; they account for up to 70%, 90% and 65% of the total received power in the intersection, congestion and obstructed-LOS scenarios, respectively. Furthermore, we find that very few MPCs stem from other traffic in the intersection and congestion scenarios. This is mainly due to the antenna

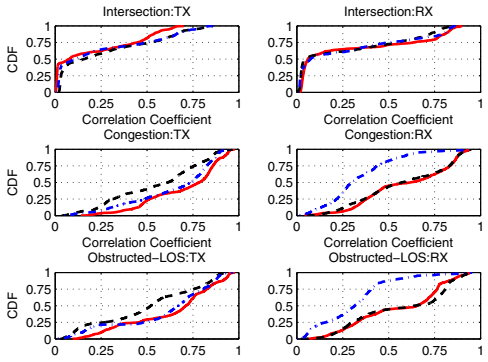

Fig. 6. Cumulative distribution function (CDF) of correlation coefficients of TX and RX antenna elements for particular separation distance d; line styles (-), (- -) and (-.) represent correlation between elements 2-1 ($d = 0.5\lambda$), 3-1 ($d = \lambda$) and 4-1 ($d = 1.5\lambda$) respectively whereas λ indicates wavelength.

arrangements we use. The mounting of the antenna close to the car roof only allows for a limited gain below the azimuth plane. Therefore, other regular (sedan-type) cars are not "seen" by the antennas.[1] Taller vehicles, on the other hand, are often found to constitute good scatterers.This is evident in the obstructed-LOS where the trucks and van surrounding the TX/RX account for the majority of the received signal.

The *azimuth direction spread* [15] is an important measure that indicates what level of spatial diversity can be anticipated. A direction spread of unity indicates that the signal arrives at the receiver uniformly spread over all directions, whereas a direction spread of zero implies that the signal arrives from a single direction. For all three scenarios, we derive the azimuth RMS direction spread at the receiver as,

$$\sigma_{\mathbf{ang}} = \sqrt{\sum |e^{j\phi_{R,l}} - \mu_{\mathbf{ang}}|^2 P_{\mathbf{ang}}(\phi_{R,l})}, \qquad (4)$$

where

$$\mu_{\mathbf{ang}} = \sum_{l=1}^{L} e^{j\phi_{R,l}} P_{\mathbf{ang}}(\phi_{R,l}), \qquad (5)$$

and $P_{\mathbf{ang}}(\phi_{R,l})$ is the normalized azimuth angular power spectrum. The direction spread is calculated with and without antenna influence and the results are shown in Fig. 5. Taking antenna influence into account, we find that the direction spread is higher in the intersection scenario because of the congested surrounding. This is in contrast to the other two scenarios where the signal is mainly composed of a small number of MPCs within a small angular range, and hence the average direction spread is low. However, the direction spread is high when removing antenna influence which encourages potential use of multi-antenna arrangements to exploit the diversity gain (see Fig. 5).

Finally, we derive the correlation coefficients between the different branches of our measured MIMO system. The correlation coefficients for both TX and RX branches are presented for all scenarios in Fig. 6. The correlation between the branches is low when there are multiple contributions from certain angles and/or there is a non-LOS condition. It is evident from Fig. 6, the correlation is low for a larger duration of time in the intersection scenario as compared to the other scenarios. This is also consistent with Fig. 5, where the intersection scenario is found to have the highest direction spread.

[1]This is particularly interesting given that the antennas were designed especially for V2V communications, with the aim of having an omni-directional antenna pattern that is maximal in the azimuth plane (given the particular position at the car roof). Readers are referred to [11] for further details.

V. Summary and Conclusions

We have presented directional analysis of Vehicle-to-Vehicle propagation channels in three different propagation environments. We found that single-bounce reflections with static objects e.g., buildings, roadsigns, and streetlights, often are the dominating propagation mechanisms in the absence of line-of-sight whereas the reflections from other vehicles contribute little unless these vehicles are tall enough. We also observe that the directional spread of the propagation channel is high, which encourages potential use of diversity-based methods.

References

[1] M. Pätzold, B. O. Hogstad, and N. Youssef, "Modeling, analysis, and simulation of MIMO mobile-to-mobile fading channels," *IEEE Trans. Wireless Commun.*, vol. 7, no. 2, pp. 510–520, Feb. 2008.

[2] A. G. Zajić and G. L. Stüber, "Space-time correlated mobile-to-mobile channels: Modelling and simulation," *IEEE Trans. Veh. Technol.*, vol. 57, no. 2, pp. 715–726, Mar. 2008.

[3] A. F. Molisch, F. Tufvesson, J. Karedal, and C. F. Mecklenbräuker, "A survey on vehicle-to-vehicle propagation channels," in *IEEE Wireless Commun. Mag.*, vol. 16, no. 6, 2009, pp. 12–22.

[4] G. Acosta-Marum and M. Ingram, "Six time- and frequency- selective empirical channel models for vehicular wireless LANs," *IEEE Veh. Technol. Mag.*, vol. 2, no. 4, pp. 4–11, 2007.

[5] I. Sen and D. W. Matolak, "Vehicle-vehicle channel models for the 5 GHz band," *IEEE Trans. Intell. Transp. Syst.*, vol. 9, no. 2, pp. 235–245, Jun. 2008.

[6] A. Paier, J. Káredal, N. Czink, C. Dumard, T. Zemen, F. Tufvesson, A. F. Molisch, and C. F. Mecklenbräuke, "Characterization of vehicle-to-vehicle radio channels from measurements at 5.2 GHz," *Wireless Personal Commun.*, vol. 50, pp. 19–29, 2009.

[7] O. Renaudin, V. M. Kolmonen, P. Vainikainen, and C. Oestges, "Non-stationary narrowband MIMO inter-vehicle channel characterization in the 5 GHz band," *IEEE Trans. Veh. Technol.*, vol. 59, no. 4, pp. 2007–2015, May 2010.

[8] M. Boban, T. Vinhoza, M. Ferreira, J. Barros, and O. Tonguz, "Impact of vehicles as obstacles in vehicular ad hoc networks," *Selected Areas in Communications, IEEE Journal on*, vol. 29, no. 1, pp. 15 –28, 2011.

[9] T. Brown, P. Eggers, K. Olesen, and G. Pedersen, "Artificial wideband multi user channels for rural high speed vehicle to vehicle links," *Selected Areas in Communications, IEEE Journal on*, vol. 29, no. 1, pp. 29 –36, 2011.

[10] J. Karedal, F. Tufvesson, T. Abbas, O. Klemp, A. Paier, L. Bernadó, and A. F. Molisch, "Radio channel measurements at street intersections for vehicle-to-vehicle safety applications," in *IEEE VTC 71*, May 2010.

[11] A. Thiel, O. Klemp, A. Paier, L. Bernadó, J. Karedal, and A. Kwoczek, "In-situ vehicular antenna integration and design aspects for vehicle-to-vehicle communications," in *EUCAP*, Apr 2010.

[12] A. F. Molisch, *Wireless Communications* $2^{nd} edition.\ IEEE Press - Wiley$, 2010.

[13] B. H. Fleury, M. Tschudin, R. Heddergott, D. Dahlhaus, and K. I. Pedersen, "Channel parameter estimation in mobile radio environments using the SAGE algorithm," *IEEE J. Select. Areas Commun.*, vol. 17, no. 3, pp. 434–450, Mar. 1999.

[14] A. Paier, T. Zemen, L. Bernadó, and G. Matz, "Non-wssus vehicular channel charachterization in highway and urban scenario at 5.2GHz using the local scattering function," in *WSA*, Feb. 2008.

[15] B. H. Fleury, "First- and second-order characterization of direction dispersion and space selectivity in the radio channel," *IEEE Trans. Inform. Theory*, vol. 46, no. 6, pp. 2027–2044, Sep. 2000.